Chapter 1

Optics on chip

It is unecessary to emphasize the importance of electronics integrated circuits to the current world. But it is worth to investigate if it is possible to create the same structure in different fields. In this investigation one can notice the two crucial feature of the success. The use of massivelly parallel device patterning enabled by photolitography and the search to decrease device size to its physical limits.

Three ramification using the microfabrication process have come of age in the last decade: Microfluidics, micro-mechanical devices (MEMs) and integrated optics. Microfluidics enables the possibility of massive chemical analysis which revolutionized genetic research, enabling operation such as DNA sequencing to be performed at a fraction of time that was done before[citation]. Micromechanical devices [weinstein thesis]. Integrated optics which has the potential of large bandwidth data transfer and spectroscopic analysis, and possibly quantum processing.

we chose integrated optics

1.1 Broad picture

The basic feature ones needs

The platform in which optic on chip works consists in the use of a high index of refraction material surrounded by a material with lower index of refraction to guide light in the higher refrative index material using the total internal reflection. We call a slab waveguide when a higher refractive index medium is cladded by a lower index medium in only dimension. Light that is guided in the higher index material can be treated a two dimensional wave. In this regime, knowledge of free space optics can be applied to design devices. Components like, lenses, mirrors, concave mirrors, prisms, gratings can be readliy visualized[citations][pictures].

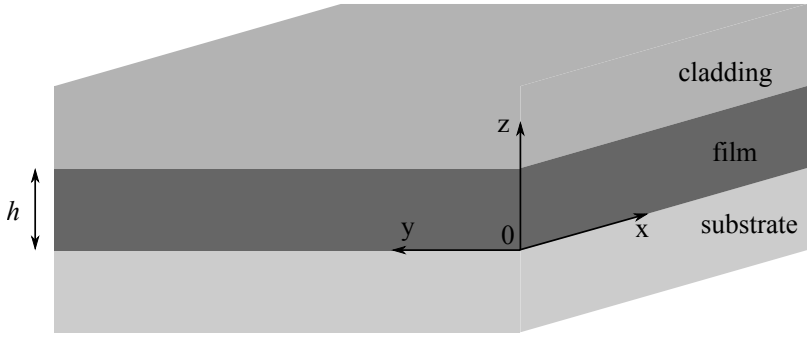

Figure 1.2.1:

Another component is wire waveguide, where a high index of refraction material is surrounded by lower index material in two dimension. This structure transport light like electrons on copper wire. This structure is widely used as fiber optics, where system built on fiber optics can implemented on chip waveguides.

In chapter we are going to dicuss the physical principles necessary to design components in integrated optics.

1.2 Slab waveguide

We define a slab waveguide as a system comprised of an infinite film (which will be also referred as core) of thicknes h and index of refraction n_f over a substrate with index of refraction $n_s$and cladded by a material whose index of refraction is n_c. As stated earlyer the index of refraction in the guiding film needs to be greater than its surroundings, this condition is stated in the relation:

$$n_f > n_s \geqslant n_c \tag{1.2.1}$$

where we left the inequality $n_s \geqslant n_c$ for sake of generallity and we take the higher index of refraction index to be the substrate.

The Maxwell equation in frequency domain for given system is:

$$\begin{aligned}
\nabla \cdot \epsilon_0 \epsilon(z)\, \mathbf{E}(\mathbf{r},\omega) &= 0 && (1.2.2)\\
\nabla \times \mathbf{E}(\mathbf{r},\omega) &= i\omega\mu_0 \mathbf{H}(\mathbf{r},\omega) && (1.2.3)\\
\nabla \cdot \mu_0 \mathbf{H}(\mathbf{r},\omega) &= 0 && (1.2.4)\\
\nabla \times \mathbf{H}(\mathbf{r},\omega) &= -i\omega\epsilon_0 \epsilon(z)\, \mathbf{E}(\mathbf{r},\omega) && (1.2.5)
\end{aligned}$$

where the net charge charge and current density was considered zero, and the permeability of the materials was considered to be μ_0. The relative dielectric constant in accordance with begining of the section is:

$$\epsilon(z) = \begin{cases} n_c^2, & \text{if } z \geq h \\ n_f^2, & \text{if } 0 < z < h \\ n_s^2, & \text{if } z \leq 0 \end{cases} \tag{1.2.6}$$

Substituing the relative dielectric constant on the Maxwell's equation we get three sets of Maxwell's equation with a constant dielectric constant:

$$\nabla \cdot \mathbf{E}_j(\mathbf{r},\omega) = 0 \tag{1.2.7}$$
$$\nabla \times \mathbf{E}_j(\mathbf{r},\omega) = i\omega\mu_0 \mathbf{H}_j(\mathbf{r},\omega) \tag{1.2.8}$$
$$\nabla \cdot \mu_0\mathbf{H}_j(\mathbf{r},\omega) = 0 \tag{1.2.9}$$
$$\nabla \times \mathbf{H}_j(\mathbf{r},\omega) = -i\omega n_j^2 \epsilon_0 \mathbf{E}_j(\mathbf{r},\omega) \tag{1.2.10}$$

where j can be either c, f or s depending on z as in 1.2.6. We can use the above equation to derive the non-coupled wave equation

$$\begin{aligned} \nabla^2\mathbf{E}_j(\mathbf{r},\omega) - k^2 n_j^2 \mathbf{E}_j(\mathbf{r},\omega) &= 0 \\ \nabla^2\mathbf{B}_j(\mathbf{r},\omega) - k^2 n_j^2 \mathbf{B}_j(\mathbf{r},\omega) &= 0 \end{aligned}$$

$$\begin{aligned} \nabla^2\mathbf{E}_j(\mathbf{r},\omega) - k^2 n_j^2 \mathbf{E}_j(\mathbf{r},\omega) = 0 \\ \nabla^2\mathbf{B}_j(\mathbf{r},\omega) - k^2 n_j^2 \mathbf{B}_j(\mathbf{r},\omega) = 0 \end{aligned}, \text{ for } j = c, f, s$$

where $k = \frac{\omega}{\sqrt{\epsilon_0\mu_0}}$. The Ansatz to the equation is a plane wave.
Using the plane wave as the ansatz
Where standard plane wave ansatz can be used

$$\psi_j = A_j \exp\left[\boldsymbol{\beta}\cdot\mathbf{R} + \kappa_j z\right]$$

where $\boldsymbol{\beta} = \beta_x\hat{x} + \beta_y\hat{y}$, $\mathbf{R} = x\hat{x} + y\hat{y}$ and

$$\beta^2 + \kappa_j^2 = n_j^2 k^2$$

where $\beta = |\boldsymbol{\beta}|$

Boundary conditions couples a set of Maxwell equations, and therefore its solutions, from one region to its neighboring region as follows:

$$\begin{aligned} \hat{z} \cdot \left(n_k^2 \mathbf{E}_k - n_j^2 \mathbf{E}_j \right) &= 0, \\ \hat{z} \cdot (\mathbf{B}_k - \mathbf{B}_j) &= 0, \\ \hat{z} \times (\mathbf{E}_k - \mathbf{E}_j) &= 0, \\ \hat{z} \times (\mathbf{H}_k - \mathbf{H}_j) &= 0, \end{aligned}$$

where k, j are either c, f or f, s and $\hat{z}$ is the unitary vector normal to the interface between different materials. Applying the boundary conditions, two sets solutions arise. Each set is characterised by the abscence of the transversal component of either electric or magnetic field. The solution which has no normal component of the magnetic field is called TM and the solutions which the normal component of the electric field are absent are called TE.

, the conditions arises

$$\tan h d_f = \frac{d_f \left(d_c + d_s \right)}{h^2 - d_c d_s}$$

$$d_j^2 = \beta^2 - k^2 n_j^2$$

1.3 Dispersion in Silicon

1.4 Rectangular waveguide

1.4.1 fem

TE-TM

1.5 Bending radius

1.6 Ring resonators

simple - add-drop - eficiency

1.7 Coupling light to the chip

1.8 Active components

1.8.1 Thermo optic effect

1.8.2 Eletrooptic effect

1.8.3 Effect χ^3

1.8.4 Plasma dispersion

1.9 Light sources

1.10 Detectors

Detector are the conversor from photonics to electronics. As with light sources the material which the detector is made of needs to be integrated to the rest of the circuit. The most used detector type relies on the excitation of electrons from the valence band to the conduction band of a semiconductor material, by the photons to be detected. But other physical effects can be used to make detector. [exemples]

Semiconductor detector, nevertheless, are the most used due to its bandwidth, limited by the electron mobility which allows bandwidth of [numbers for]. Sensitivity, (operating in avalanche mode single photons can be detected). Simplicity, in metal-semiconductor-metal (MSM) the only thing needed is the detecting semiconductor material and the metal contacts. Depoing the endpoints of the detector creating a PIN structure will allow eliminate the need for an external voltage drive.

Two materials are most commonly used. Germanium and Indium Galium Arsenide (InGaAs)

1.11 Fabrication Tecniques

Chapter 2

Diffraction Grating Spectrometers

It is difficult to enumerate all the contribuition to society that diffraction grating has brought. Its role on identifying the discrete energy levels of atoms provided a significant amount of information to the development of quantum mechanics. Currently its use in the identification or quantification of chemical compounds and its structure constitutes the majority usage end of diffraction gratings.

Historically, diffraction grating spectrometers have been builky table top devices. But sizes have been decreasing, and handheld devices are already comercialized. Further in the chapter we will discuss how the devices is limited. Because of its role in chemical analysis this device would...

Diffraction grating spectrometers can be integrated on chips, and this type of devices have been manufactured for wavelength demultiplexing devices in the telecomunication industry.

2.1 Kirchhoff's diffraction theory

$$U(P) = -\frac{iA}{2\lambda}\iint_A \frac{e^{ik(r+s)}}{rs}\left[\cos(n,r) - \cos(n,s)\right] dS \tag{2.1.1}$$

For aperture much smaller then r and s then, putting the origin somewhere in the aperture

$$U(P) \sim -\frac{Ai}{\lambda}\frac{\cos\delta}{r's'}\iint_A e^{ik(r+s)}, \tag{2.1.2}$$

where

$$U(p,q) = \iint G(\xi,\eta)\exp\left[-\frac{2\pi}{\lambda}(p\xi + q\eta)\right] d\xi d\eta,$$

where G is the pupil function.

$$U(p,q) = C\sum_n \iint_A e^{-ik[(\xi_n+\xi')p+(\eta_n+\eta')q]} d\xi' d\eta'$$

or

$$U(p,q) = C\sum_n e^{-ik(\xi_n p+\eta_n q)} \iint_A e^{-ik(\xi' p+\eta' q)} d\xi' d\eta'$$

2.2 Diffraction grating

A diffraction grating may be defined as any arrangement which imposes on an incident wave a periodic variation of amplitude of phase, or both. We may characterize any particular grating by its *transmission function*, defined as follows:

Let a transparent or semitransparent object (not necessarily periodic) cover a portion of a fictitious reference plane $\xi\eta$, and let it be illuminated by a plane monochromatic wave incident in a direction specified by the direction cosines l_0, m_0. Fig illustrates the arrangement, the η-axis being perpendicular to the plane of he drawing. If no object were present, the disturbance in the ξ, η-plane would be represented by the function $V_0(\xi,\eta) = A\exp[ik(l_0\xi + m_0\eta)]$, the factor $\exp(-i\omega t)$ being, as usual, omitted. Because of the presence of the object disturbance will be modified and may be represented by some other function, which we denote by $V(\xi,\eta)$. The *transmission function* of the object is then defined as

$$F(\xi,\eta) = \frac{V(\xi,\eta)}{V_0(\xi,\eta)}.$$

In general F depends, not only on ξ and η but also on the direction (l_0, m_0) of illumination. The transmission function is in general complex, since both the amplitude and the phase of the light may be altered on the passing through the object. In the special case when the object alters the amplitude but no the phase of the incident wave (i.e. if $\arg F \equiv 0$), we speak of an *amplitude object*; if it alters the phase but not the amplitude (i. e. $|F| = 1$) we speak of a *phase object*.

If we are concerned with reflected light rather than with light that is transmitted by an object, it is more appropriate to speak of a *reflection function*, defined in a similar way, the only difference being that the reference plane is on the same side of the object as the incident light.

The ratio $|V/V_0|$ is practically unity for points outside the geometrical shadow (whose boundary is represented by points A and B in Figure) cast by the object. If the portion outside the shadow region is covered by an opaque screen, the arrangements act as a diffracting aperture A with a nonuniform pupil function. ~~If the linear dimensions of A are large compared to the wavelength and if F remains sensibly constant over regions whose dimensions are of the same order as the wavelength, the diffraction formula remain valid under the same conditions as before, provided that the integrand of the diffraction integral is multiplied by F.~~

Let us now consider a one-dimensional grating consisting of n parallel grooves of arbitrary profile,

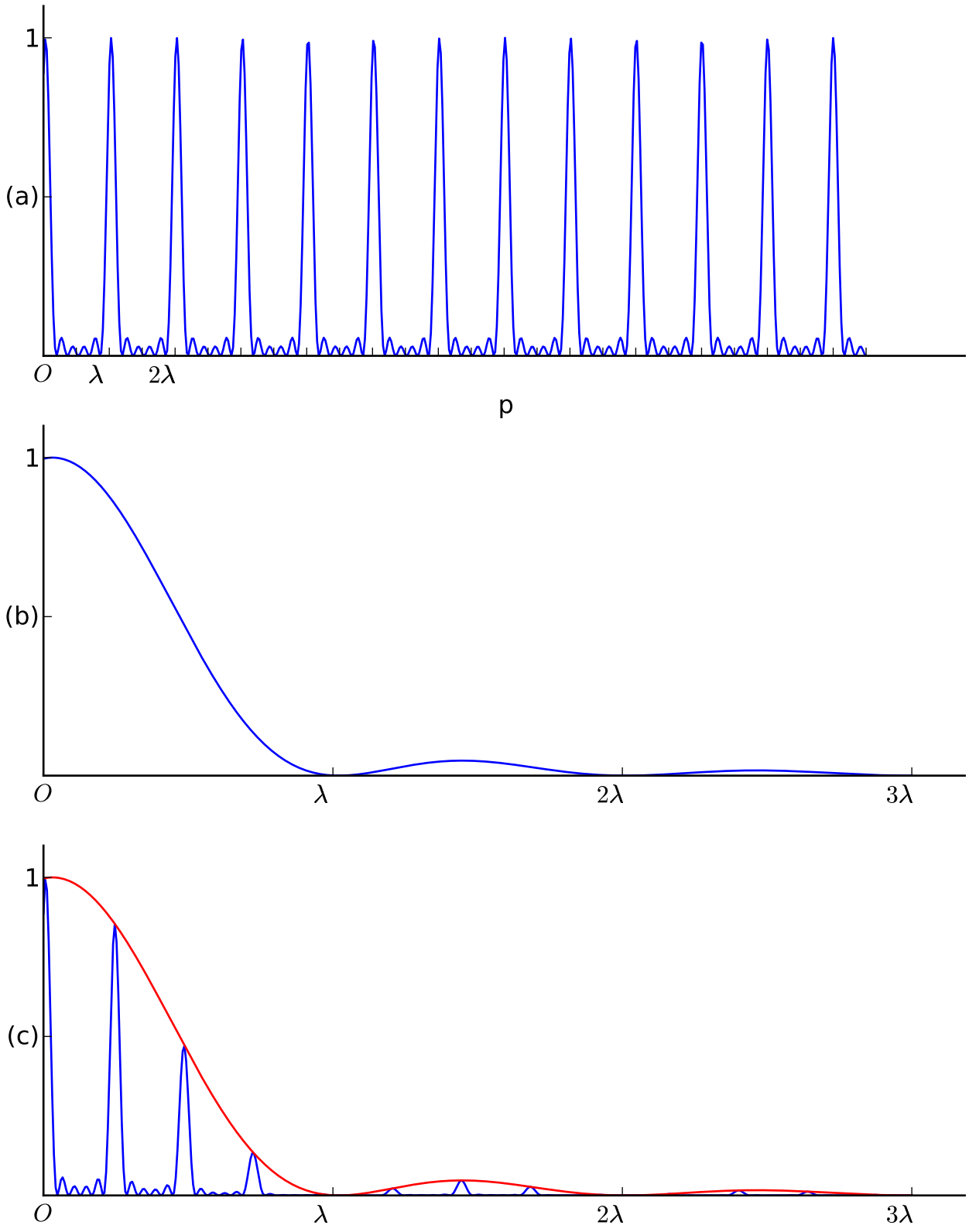
1
(a)
O
λ
2λ
p
1
(b)
O
λ
2λ
3λ
1
(c)
O
λ
2λ
3λ

ruled on one surface of a plan-parallel glass plate. Let the ξ, η-plane coincide with the plane face of the plate, η being the direction of the grooves and let d be the period in the ξ direction.

Assume that the direction of propagation of the wave incident upon the grating is in the plane of the figure, making an angle θ_0 with $O\zeta$, and let θ denote the angle which $O\zeta$ makes with the line joining a very distant point of observation P with the grating.

As before we set $l_o = \sin\theta_0$, $l = \sin\theta$, $p = l - l_0 = \sin\theta - \sin\theta_0$. The complex amplitude at P is then immediately obtained from, where the integrand must be multiplied by the transmission function F of one periodic element. We may set $q = 0$ and

$$\xi_n = nd, \quad \eta_n = 0 \quad (n = 0, 1, \ldots, N-1) \ .$$

We the obtain

$$U(p) = U^{(0)}(p) \sum_{n=0}^{N-1} e^{-iknd p} = U^{(0)}(p) \frac{1 - e^{-iNkdp}}{1 - e^{-kdp}}, \tag{2.2.1}$$

where

$$U^{(0)}(p) = C \int_A F(\xi)\, e^{-ikp\xi}\, d\xi. \tag{2.2.2}$$

Hence

$$I(p) = |U(p)|^2 = \frac{\left(1 - e^{-Nkdp}\right)}{(1 - e^{-kdp})} \cdot \frac{\left(1 - e^{Nkdp}\right)}{(1 - e^{kdp})} \left|U^{(0)}(p)\right|^2 = \frac{1 - \cos Nkdp}{1 - \cos kdp} I^{(0)}(p)\,,$$

where $I^{(0)}(p) = \left|U^{(0)}(p)\right|^2$. If we introduce the function

$$H(N, x) = \left(\frac{\sin Nx}{\sin x}\right)^2,$$

the formula 5 for the intensity may be written as

$$I(p) = H\left(N, \frac{kdp}{2}\right) I^{(0)}(p)\,.$$

Before discussing the implications of this basic formula we note that according to 2.2.1. The light distribution is the same as that due to a set of coherent secondary sources each characterized by the same amplitude function $\left|U^{(0)}(p)\right|$ and with phases that differ form each other by integral multiples of kdp. To see the significance of this phase difference consider two corresponding points A and B in the neighboring grooves of the grating. Since the effect of the grating is to impress a periodic variation onto the incident wave, it follows that the path difference between the light arriving a A and at B is the same as in the absence of the grating, i.e. it is equal to $AK = d\sin\theta_0$,

K denoting the foot of the perpendicular from B on to the ray incident at A. Further, the light path from B in the direction θ exceeds the light path from A by $BL = d\sin\theta$, L being the foot of the perpendicular from A on to the ray diffracted at B in the direction θ. Hence the total path difference between light arriving at the distant point of observation form corresponding points in two neighboring grooves is

$$BL - AK = d\left(\sin\theta - \sin\theta_0\right) = dp, \tag{2.2.3}$$

and the corresponding phase difference is $2\pi dp/\lambda = kdp$.

Formula expresses $I\left(p\right)$ as the product of two functions: one of them, $I^{(0)}$, represents the effect of a single period of the grating; the other, $H\left(N,x\right)$ has maxima, each of height N^2 when

$$p \equiv \sin\theta - \sin\theta_0 = \frac{m\lambda}{Nd}\left(m = 0, \pm1, \pm2, \ldots\right), \tag{2.2.4}$$

The integer m represents, according to 7, the path difference in wavelengths between light diffracted in the direction of the maximum, from corresponding points in two neighboring grooves. In agreement with our earlier definition,7.3.1, we call m the *order of interference*. Between theses principal maxima there are weak secondary maxima (see fig 8.19a), the first secondary maximum being only a few percent of the principal maximum when N is large. The maxima are separated by points of zero intensity at $x = kdp/2 = \pm n\pi/N$, i.e. in directions given by

$$p \equiv \sin\theta - \sin\theta_0 = \frac{n\lambda}{Nd}\left(n = 0, \pm1, \pm2, \ldots\right) \tag{2.2.5}$$

the case where n/N is an integer being excluded.

The function $I^{(0)}\left(p\right)$ depends on the form of the grooves. Suppose that it has principal maximum for some direction $p = p'$ and that on both sides of the maximum if falls off slowly in comparison with H. Then $I\left(p\right)$ will have the general form o the sharp maxima near the directions $p = m\lambda/d$. Since these directions (except for $m = 0$) depend on the wavelength, we see that the grating will decompose a beam of non-monochromatic light into *spectral orders*.

To illustrate these remarks let us consider a grating consisting of a succession of long equidistant slits, each of width s and length L, in an opaque screen. If the grating is illuminated from a very distant line source parallel to the slits, the intensity $I^{(0)}$ is given by the expression 2.2.2 (with $2a = s$, $2b = L$) and we obtain

$$I\left(p\right) = \frac{sE}{\lambda R^2}\left(\frac{\sin\frac{Nkdp}{2}}{\sin\frac{kdp}{2}}\right)^2\left(\frac{\sin\frac{kdp}{2}}{\frac{kdp}{2}}\right)^2. \tag{2.2.6}$$

Curves representing the two factors in 2.2.6 and their product are shown in fig X. The last factor

in 2.2.6, which represents the effect of a single slit, has a principal maximum at $p = 0$ and minima given by $ksp/2 = n\pi$, i.e. at

$$p = \frac{n\lambda}{s}, (n = 0, \pm 1, \pm 2, \ldots)$$

separated by weak secondary maxima. We see that if $\lambda/s \gg \lambda/d$, i.e. if the width of each slit is small compared to d, the intensity $I(p)$ has in addition to a principal maximum at $p = 0$ a series of sharp, but progressively decreasing, maxima on either side of it, near direction given by 2.2.4.

Returning to the general case, it is evident that if the width of each groove is very small, of the order of a wavelength (as is often the case in practice) the formula derived on the basis of Kirchhoff's approximation, can evidently no longer be expected to hold. In such cases more refined considerations must be make to determine the detailed distribution of the intensity. We may, however, expect that the main qualitative features indicated by our elementary theory, namely the existence of sharp maxima whose positions are substantially determined by the interference function H, remain even when the grooves are very narrow, provided, that the intensity function of a single period varies slowly in an interval of the order $\Delta p = \lambda/d$. Let us now consider the resolution that may be attained with a grating. The separation between a primary maximum of order m and a neighbouring minimum is, according to 2.2.5, given by

$$\Delta p = \frac{\lambda}{Nd}.$$

If the wavelength is changed by an amount $\Delta\lambda$, the mth-order maximum is according to 2.2.4, displaced by an amount

$$\Delta' p = \frac{|m|}{d}\Delta\lambda.$$

Assuming that the lines of wavelength $\lambda \pm \frac{1}{2}\Delta\lambda$ will just be resolved when the maximum of the one wavelength coincides with the first minimum of the other we have on he limit of resolution in the mth order, $\Delta p = \Delta' p$, i.e.

$$\frac{\lambda}{\Delta\lambda} = |m| N. \tag{2.2.7}$$

Thus, *the resolving power is equal to the product of the order number m and the number N of the grooves*. For the mth order we have, according to, that $d(\sin\theta - \sin\theta_0) = m\lambda$, so that we may also express the resolving power in the form

$$\frac{\lambda}{\Delta\lambda} = \frac{Nd\,|\sin\theta - \sin\theta_0|}{\lambda}.$$

Because of 2.2.3 this implies that *the resolving power is equal to the number of wavelengths in the path difference between rays that are diffracted in the direction θ from the two extreme ends*

(separated by distance Nd) of the grating. It is to be noted that since $|\sin\theta - \sin\theta_0|$ cannot exceed 2, the resolving power that can be attained with a grating of overall with w can never exceed the value $2w/\lambda$.

2.2.1 Free spectral range

From the resolving power equation 2.2.7, we conclude that spectrometer should be operated on high diffraction order so as to minimize the device size for a given resolution. Unfortunatelly, the grating equation 2.2.4, $p \equiv \sin\theta - \sin\theta_0 = \frac{m\lambda}{Nd}$, we see that it is possible for light from to different wavelength in differente diffraction orders to be diffracted to the same angle θ, sufficing that

$$m_i\lambda_i = m_j\lambda_j$$

for $i \neq j$, so for example light diffracted in order 1 at wavelength 1500 nm is diffracted in the same direction as light diffracted from order 2 wavelength 750 nm. To avoid this ambiguity, it is of interest to know when this condition happens. From the grating equation we see that p does not make sense outside the interval [0,1], therefore, $0 \leq \frac{m\lambda_m}{Nd} \leq 1$ we then that for the diffraction order m the wavelength range that is going to be diffracted is:

$$0 \leq \lambda_m \leq \frac{Nd}{m}.$$

So for the first order the wavelength range that exists is every wavelength below Nd , for order 2 every wavelength below $Nd/2$ and so on. We see then, that for order 1 the range $[Nd, Nd/2]$ is occupied solely by order one. For order 2 the range $[Nd/2, Nd/3]$, for order m, $[Nd/m, Nd/(m+1)]$. We see that the range width $\Delta\lambda_m$ which there is no overlaping diffraction, called *free spectral range*, can be computed as

$$\Delta\lambda_m = \frac{Nd}{m} - \frac{Nd}{m+1} = \frac{Nd}{m(m+1)},$$

we can replace the substitute the dependancy on Nd for the wavelength in the center of the free spectral range λ_{Cm},

$$\lambda_{Cm} = \frac{Nd}{m} - \frac{\Delta\lambda_m}{2} = \frac{Nd}{m(m+1)}(m+0.5),$$

It is worth noting that althought λ_{Cm} is in the middle of the spectral range $\Delta\lambda_m$ the wavelenths are not linearly distributed along the angle range that it is diffracted to, and therefore λ_{Cm} is not located at the center of the angle range of the mth order free spectral range. [Graph]We see then

that the free spectral range depends inverselly with the diffraction order used,

$$\Delta\lambda_m = \frac{\lambda_{Cm}}{m + 0.5}. \tag{2.2.8}$$

This fact, ties to use the a maximum operating diffraction order to the wavelength range and central wavelength we want the diffraction grating to operate.

2.3 Planar devices

The previous exposition on diffraction grating does not change on the medium in which the device is built on. But since we are interested in spectrometeres integrated on chips, it worth lifting the characteristics of this device. From this point two features stand out as very different from regular free space spectrometer. First is that light is always guided in a slab waveguide, the confinement of light in one dimension change the nature of the system from a 3 dimensional to bi-dimensional one. As this fact causes the light power to decay with the inverse of the distance as it moves away from the source. The other diference is the change of the dispersion due to both the material and the confinement effect. The outcome of this is that for all the results in the previous section, the wavelength variable that needs to be considered is the effective wavelenght in the medium.

$$\lambda_{\text{eff}} = \frac{\lambda}{n_{\text{eff}}}$$

2.4 Spectrometer Architectures

Several architecture to build diffraction grating spectrometer exists. Due to lowest size resolution of the Rowland design, it was chosen to build the spectrometer. The Czerny-Turner is presented here to introduce spectrometer because its design is easily understandable. Arrayed waveguide grating has been the most used planar (on chip) version of spectrometer. Marketed as wavelength de-multiplexer (WDM) this layout is show because its role in the telecommunication industry it is of interest to understand why it is not fit for role high resolution on chip spectrometer.

2.4.1 Czerny-Turner

Due to its modularity this architecture is probably the best to introduce spectrometers. It is composed of two slits, two concave mirrors and a diffraction grating. As shown in figure 2.4.1, the light to be analyzed is shined through the entrance slit. Due to diffraction, the light fan out as it propagates to the collimating concave mirror where light is collimated and reflected in the

direction of the diffraction grating. The diffraction grating then, deviates light from each different wavelength (optical frequencies) into different angles following the equation 2.2.4. A focusing concave mirror focus the light coming from the diffraction grating and deflect it to the detector slit.

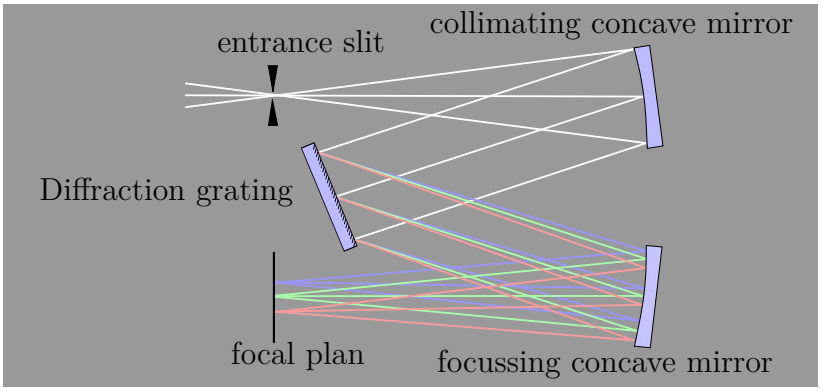

Figure 2.4.1: Czerny-Turner architecture

The function of the entrance slit is to filter spatial optical modes that are inputed into the system. For best filtering the slit has to transmit only a single spatial mode. This is achieved by making the slit width of the order of the light wavelength. Decreasing slit width will increase the beam spread angle, as depicted in figure 2.4.2, for a chosen final beam width this will allow the collimating concave mirror to placed nearer to the slit decreasing the device size. However, decrease the slit width will also decrease the fraction of transmitted light. and therefore, lowering the device sensitivity.

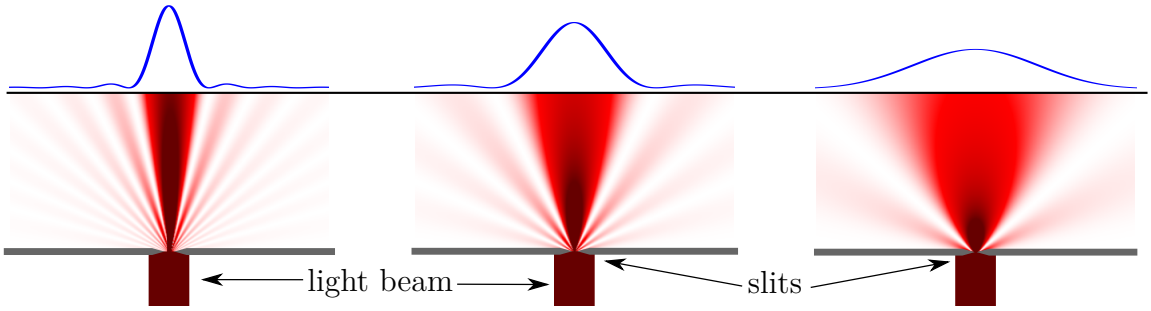

Figure 2.4.2: Different effects of slit width

As described by its name the collimating concave mirror collimates the light coming from the entrance mirror and redirect it to the diffraction grating. In order to collimate the input light, the curvature radius should be equal twice the distance from the entrance slit to the center of the collimating concave mirror. The mirror diameter must be bigger than the beam width at the when it arrives at it to avoid losing light power.

The diffraction grating deviates light from each different wavelength into different angles, as described by equation 2.2.4. Details on how the light is diffracted are explained in section 2.2. Roughly, the number of illuminated grooves, which is equal to the beam diameter divided by the groove pitch, will determine the resolving power of the spectrometer, as shown in equation 2.2.7.

To quantify the amount of light deviated to each different direction, we use a focusing concave mirror, which will map light with different direction and focus them each into a distinct point in a plane. Alternatively we can say that light in different k in the k space into different points in the coordinate space. Clearly, the size of the focusing mirror must be such that it collects most of the light coming from the diffraction grating. This means that it must be bigger than the beam size plus account for the spread of different wavelengths.

A detector is placed at a point in the focus plan to measure the light power. Optimum detector size is of the order of the entrance slit width, limited also by the resolving power of the diffraction grating. Placing a exit slit in the focus plane followed by a detector, can be used as an alternative for the slit size detector.

Figure 2.4.3: Detector array and slit and detector options

Size analise

2.4.2 Rowland

In year, Rowland [3] found a way to incorporate the collimating and focusing elements into the diffraction grating. This layout not only decreased the final device size, but also eliminate spherical and astigmatism aberrations due to the auxiliary concave mirrors.

The design consists in the use of a concave diffraction grating of radius 2R. The entrance and exit slits positions are located in a circle of radius R tangent to the diffraction grating sphere. Or more precisely tangent to one of the equator of the diffraction grating sphere. For optimum area usage, the equator should be perpendicular to the diffraction grating grooves and passing through the grating center.

2.4.3 Arrayed Waveguide Grating (AWG)

The resolving power of a diffraction grating is proportional to the number of grooves and diffraction order, as shown in equation 2.2.7. Diffraction grating based on ruled surfaces can not achieve diffraction order greater than 20. Introduced by Takahashi et. al.[4], this limitation can be overcome by replacing the grating grooves by an array of waveguides. To understand how the introduction of waveguide help it is necessary to understand more generally what diffraction order is.

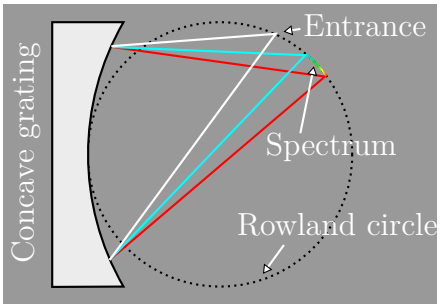

Figure 2.4.4: Rowland design.

We say that certain diffraction peak is of order m if each wave from the set that was constructively interfered to form the interference peak is delayed from one another of m periods. On traditional ruled surface diffraction gratings, wavefront from different period are made to interfere by making the wave travel different path lengths by taking path that deviates from the equal angle reflection.

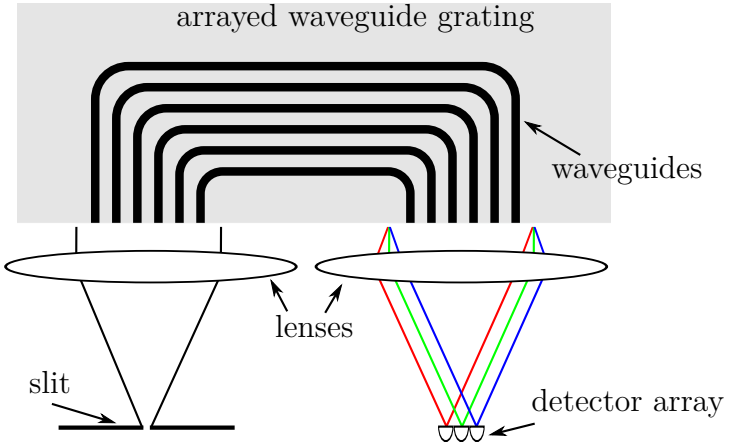

Figure 2.4.5: Traditional diffraction grating generate different path length by straying away from equal angle reflection.

By guiding light through waveguide it is possible to increase the difference of path length among different waveguides, achieved by only changing the waveguides lengths. Each waveguide of the waveguide array would function like a groove in the diffraction grating, but since waveguide length is only limited by its intrinsic loss, the difference of path length can be on the order of hundreds of wavelength, giving raise to grating that operate of diffraction order of also hundreds.

Unfortunately there is a drawback of increasing diffraction order, the free spectral range as described in 2.2.8, decreases with the inverse of the of the diffraction order. For instance, an arrayed waveguide grating working on diffraction order 100 at wavelength 1500 nm would have a FSR of only 15 nm. Although this range is useful for fiber optics telecommunications, this bandwidth is too small for most spectroscopy application, optical coherence tomography or ultra-fast oscil-

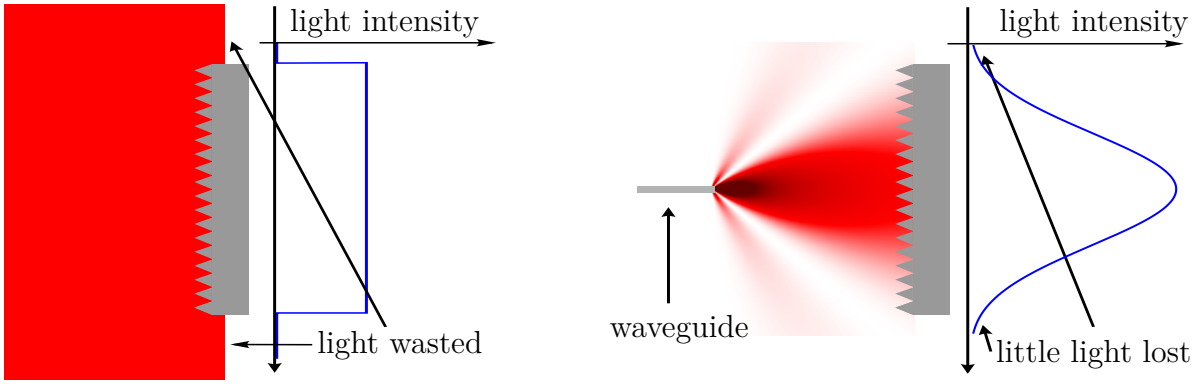

Figure 2.5.1:

loscope[refs]. Since we want to achieve a wide spectrum range, this architecture is not fit for us.

2.5 Grating illuminated by a Gaussian Beam

On section 2.2, it was assumed that the whole grating was uniformly illuminated. In practice, this case not always occurs. Light source is normally a collimated light from a slit, pin hole or fiber optics, where for best resolution, single mode output should pass through. In those cases the tranversal power profile is better modeled by a gaussian than by a square profile, see figure 2.5.1. To ajust the resolving power equation 2.2.7 to account for the Gaussian profile illumination we have to alter the squared illumination assumption in equation 2.2.1. Using the relation we can equate

$$U(p) = U^{(0)}(p) \int \sum_{n=-\infty}^{\infty} \delta(x-n)\,\mathrm{rect}\left[\frac{x}{2(N-1)}\right] e^{-ikxdp} dx$$

where

$$\mathrm{rect}(x) = \begin{cases} 0 & \text{if } |x| > \frac{1}{2} \\ \frac{1}{2} & \text{if } |x| = \frac{1}{2} \\ 1 & \text{if } |x| < \frac{1}{2}. \end{cases}$$

the rect(x) function correspond to the squared illumination assumption, for a Gaussian illumination we simply replace tha function by a Gaussian function

$$\mathrm{gauss}(x) = \exp\left[-4\ln 2\left(\frac{x}{w/d}\right)^2\right]$$

where d is the grating pitch, and w is the Full Width at Half Maximum of the illuminating beam at the grating. Replacing the Dirac delta comb by its Fourier series

$$\sum_{k=-\infty}^{\infty} \delta\left(x-k\right) = \sum_{m=-\infty}^{\infty} e^{i2\pi mx},$$

we get

$$U\left(p\right) = U^{(0)}\left(p\right) \sum_{m=-\infty}^{\infty} \int \exp\left[-4\ln 2\left(\frac{x}{w/d}\right)^2\right] e^{-i2\pi x(kdp/2\pi - m)} dx$$

performing the integral we obtain a comb of Gaussian

$$U\left(p\right) = U^{(0)}\left(p\right) \frac{w}{\sqrt{2}} \sum_{m=-\infty}^{\infty} \exp\left[-\frac{1}{4}\left(\frac{kdp}{2\pi} - m\right)^2 \frac{\left(w/d\right)^2}{4\ln 2}\right], \tag{2.5.1}$$

where each Gaussian is centered on the diffraction order m. From it we get

$$\frac{kdp}{2\pi} = m \text{ or } p = \frac{\lambda m}{d}. \tag{2.5.2}$$

From equation 2.5.1 we can define the wavelength width $\Delta\lambda$ such that the power of wavelength λ at diffraction order m, is halven as a been

$$\Delta p = 2\ln 2 \frac{\lambda}{w},$$

or using the grating equation 2.5.2 e define the resolving power for a gaussian beam illuminated diffraction grating as

$$\frac{\lambda}{\Delta\lambda} = 2\ln 2 \frac{wm}{d} \tag{2.5.3}$$

2.6 Size

For a given wavelength λ, resolution $\Delta\lambda$ and free spectral range $\delta\lambda$, one would like to minimize the device size. Since the device size is basically defined by the grating size W. We have $W = a\frac{\lambda^2}{\Delta\lambda}$. Since $Nm = \frac{\lambda}{\Delta\lambda}$. $W = a\frac{\lambda m}{\Delta\lambda}d$, $\delta\lambda = \frac{\lambda}{m}$. $W = a\frac{\lambda^2}{\delta\lambda\Delta\lambda}d$

2.7 Spectral defects

2.7.1 Rowland Ghosts

Rowland ghosts are spurious lines seen in some grating spectra that result from periodic errors in the spacing of the grooves. These are usually located symmetrically with respect to each strong spectral line at a spectral distance from it, which depends on the period of the error, and with an intensity that depends on the amplitude of this error.

2.7.2 Lyman Ghosts

2.8 Aberrations

The resolving power equation 2.2.7 states that the resolution of a diffraction grating depends linearly with the wavelength. Unfortunatelly, that relation is only valid for plane waves. To use segregation capability of the diffraction grating, it is necessary to have a source of plane waves and to measure the light power that go to different direction after diffraction from the grating. Sources and detector are space localized endpoints. But employing lenses, it is possible to convert a space localized mode to a angle localized mode., as discussed on the Czerny-Turner configuration in section 2.4.1. This conversion, however, is not perfect. In geometrical optics terms, this means that rays that enter parallel in a lens (or any other focusin device) does no converge to a single point after the lens and with the fase arriving at exaclty the same time(picture?). Integrating the lens into the grating, as done in Rowland configuration in section 2.4.2, does not readily eliminate the problem, but its application together with the potencial to fabricate designs with freedom to choose any geometry and dispersion might be the solution.

First we will state formally what conditions need to be satified in the design of a aberration free spectrometer. The non-existance of a mathematical solution, lead us to show two corrections, named one point and two point stigmatic correction, that reduce aberrations.

2.8.1 Aberration free conditions

One would like to design a perfect spectrometer free of aberration. The ability of electron beam lithography to define with accuracy of nanometers the position and shape of the grating grooves.

The problem can be stated as follows: Light coming from a point I fan out to a diffraction grating which the i-th groove, of N grooves, is located at G_i, at each groove light is reflected, fans out again and propagates to a set of M output waveguides which the j-ith waveguide is located at O_j,

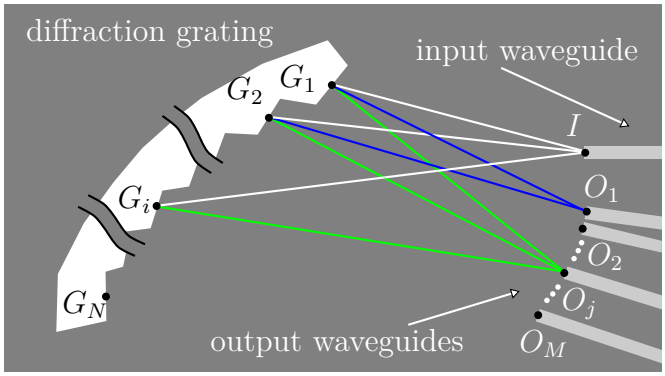

Figure 2.8.1:

as shown in figure 2.8.1. To perfectly separate light from different wavelengths, we would like that all light which has wavelength λ_j coming from each groove arrive in phase at the output point O_j. Furthermore, we would like that light coming from each different groove have be in a different cycle. The previeous conditions can be expressed by a system of $N \times M$ nonlinear algebraic equations with the prototype

$$\overline{IG_i} + \overline{G_iO_j} = \lambda_j \left(a_j + mi\right) \text{ for } \left(i = 1, 2, \ldots, N\right) \text{ and } \left(j = 1, 2, \ldots, M\right), \tag{2.8.1}$$

where m is an integer number which defines the diffraction order and a_j is a constant that states that the absolute path length does not matter, only the path length difference between light coming from different routes do. It is worth emphasizing that the path length evaluation should consider the medium refractive index, from this perspective one can interpret that light is also propagating in a non-euclidean space.

For the case of a flat space in a plane, equation 2.8.1 can be expanded to

$$\sqrt{\left(I_x - G_{ix}\right)^2 + \left(I_y - G_{iy}\right)^2} + \sqrt{\left(O_{jx} - G_{ix}\right)^2 + \left(O_{jy} - G_{iy}\right)^2} = \lambda_j \left(a_j + mi\right) \text{ for } \left(i = 1, 2, \ldots, N\right) \text{ and } \left(j = 1, 2 \right. \tag{2.8.2}$$

As discussed in sections 2.2 and 2.5, high resolution implies in the use of a high number of grooves N with numbers tipically achieving, thousands to millions. Number of channels M is, of course, as a wish of the costumer but numbers around thousands are very typical. These implies that the set of equations 2.8.2 is comprised of $M \times N$ equations with and $2N + 2C + 1$ variables

All equation

show that there is no build the full set of equations

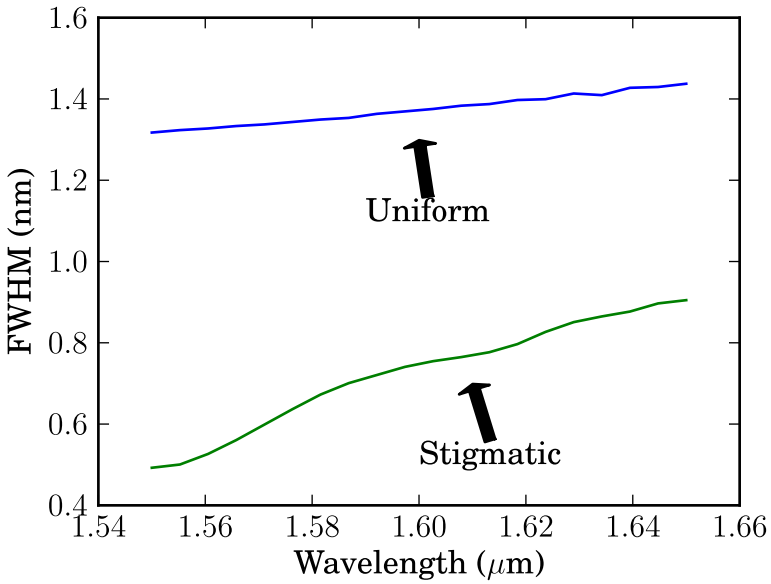

Figure 2.8.2:

cite the papers that show it is not possible to solve for Euclidean surface, but nothing has been shown for non-Euclidean surfaces. Fabrication of non-Euclidean surfaces have been used to demonstrate cloaking devices[2]. Although it is not possible to find a solution for all equations, solving for one and two points dramatically improves aberration.

2.8.2 One point stigmatic correction

In the modality a degree of freedom is left undefined leaving us the possibility to choose the surface in which the diffraction grooves are going to be positioned. Using the Rowland design as a basis, we show here how to place the grooves on a circle in order to have a wavelength free of aberration.

2.8.3 Two points stigmatic correction

2.9 Blazing and Groove size

2.10 Rayleigh-Huygens model

Numerical calculation where carried out using a Rayleigh-Huygens method adapted to a bidimensional world[1]. The implementation was done in a Python script program. And the program is available at http://code.google.com/p/khsimulator/.

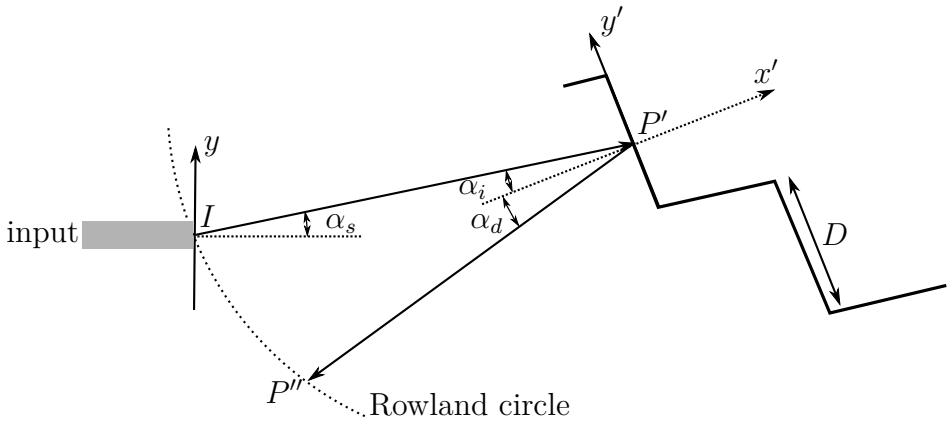

Figure 2.10.1:

According to the Kirchhoff-Huygens diffraction formula, the incident electric field E_{inc} at the center points of the grating facets (P') at a distance $r_1$and at an angle α_s can be calculated as

$$E_{\text{inc}} = \frac{1}{2}\sqrt{\frac{n_{\text{eff}}}{\lambda}} \int E_{\text{wg}}(y) \frac{e^{-jkr_1}}{\sqrt{r_1}} (1 - \cos\alpha_s)\, dy$$

where $k = 2\pi n_{\text{eff}}/\lambda$ is the wavenumber within the slab waveguide, and E_{wg} is the electric field profile of the TE-polarized fundamental mode of the input waveguide. Similarly, the diffracted field E_{out} on the collection wavguides is calculated as

$$E_{\text{out}}(P'') = \eta\sqrt{\frac{n_{\text{eff}}}{\lambda}} \sum_{\text{Grating}} \int_{-D/2}^{+D/2} E_{\text{inc}}(y) \frac{e^{-jkr_2}}{\sqrt{r_2}} \frac{(\cos\alpha_i - \cos\alpha_d)}{2} dy'$$

where α_i and α_d are the incident and diffracted angles with respect to the normal of each grating facet, and η is the reflection coefficient of the grating. This formula is simplified if we assume that the magnitude of the incident field $|E_{\text{inc}}|$is constant over each facet and the pahse of this field changes linearly along the length of the facet

$$E_{\text{inc}}(y') = E_{\text{inc}}(y' = 0)\, e^{+iky' \sin\alpha_i}.$$

This aaproximation is valid if the sie of the facets is small compared with the distance to the input and if thangle of incidence α_i is small. This is thye case if the blaze point (O) is positioned near the input waveguide (I).

2.11 Comparisons of simulationas and analitic solution

2.12 Simulation of Spectral defects and aberrations using Rayleigh-Huygens model

2.13 implementation

The integration of silicon photonics and electronics in a CMOS compatible platform enables whole monolithic device such as a wavelength division demultiplexer (WDM) integrated with detectors and electronic amplifiers. Most silicon-on-insulator (SOI) WDMs with 1 nm channel spacing typically cover a spectral range of only 10 nm. The small spectral range in typical WDMs is due to the use of arrayed waveguide grating (AWG)[1,2] designs where large grating orders are employed to achieve small channel spacing which comes with the cost of free spectral range. It is possible to increase the spectral range by lowering the grating order and adding more waveguides to compensate, but this increases the overall chip size. Furthermore, due to the high index contrast of the silicon photonics platform, the achievable resolution depends on very fine control of the AWG waveguide dimensions. Here we demonstrate WDM using etched diffraction grating (EDG)[3-5]. This design is more fabrication tolerant since light is propagating in a slab where the only dimension that needs to be controlled is the slab thickness. It is also more suitable to work at a low grating order because light diffracts in a single slab opposed to the two star couplers slabs in the AWG.

2.13.1 Design

We designed a WDM that uses a Rowland design with one stigmatic point correction. The system was designed so that stigmatic point was located at the central waveguide of the 21 output waveguide array. The central wavelength was chosen to be 1500 nm and the diffraction order was 10. The Rowland circle was chosen to be 750 μm. The designed grating contains 340 grooves. The resulting free spectral range was estimated to be 117 nm, and the groove spacing approximately 4 μm. The input and output waveguide apertures were 1.4 μm. A reference waveguide was placed next to the spectrometer so that the transmission efficiency could be estimated.

2.13.2 Fabrication

We fabricated the device using CMOS compatible procedures. First, we start with an SOI wafer with 250 nm silicon and 3 μm buried oxide. An 80 nm layer of SiO2 was deposited using plasma

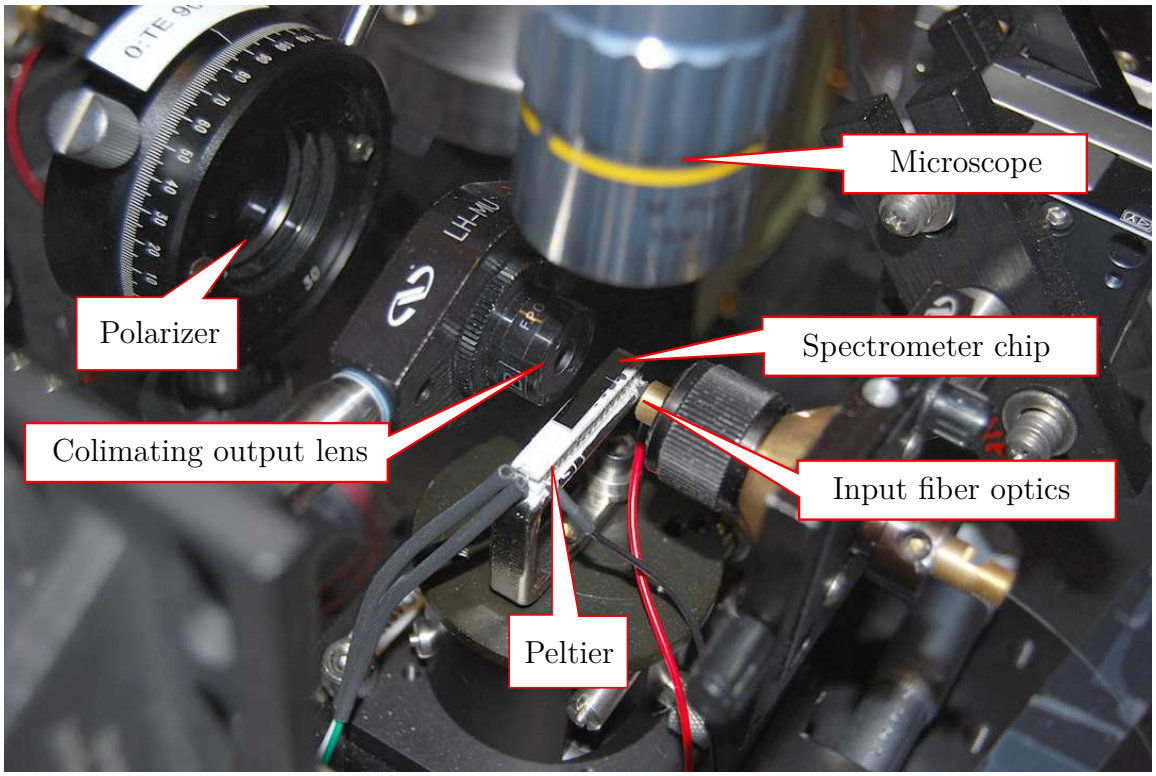

Figure 2.13.1:

enhanced chemical vapor deposition (PECVD) to be used as a hard mask. A 200 nm layer of PMMA was spun and then the grating and the waveguides were defined using e-beam lithography. The pattern was transferred from PMMA the to the oxide layer using CHF3/O2 reactive ion etch. The silicon layer was etched using Cl2 inductively coupled plasmaand then 2.3 μm of SiO2 was deposited using PECVD to clad the device. The wafer was diced and polished for optical testing.

2.13.3 Testing

Testing setup photo

We measured the performance of our WDM and observed -10 dB crosstalk and 1 nm channel spacing across 21 channels. As shown in Fig. 2, a relatively flat transmission spectrum was obtained. This result was measured by inserting light from a tunable laser and measuring the power from the output waveguides. A fiber polarization controller was used to set the input polarization to TE and a polarizer was placed between the chip output and the detector to filter out any TM polarized light. An insertion loss of -10 dB was estimated by comparing to the transmission through the reference waveguide. This can be attributed to Fresnel reflection between the Si-SiO2 interfaces at the grating groove facet and can be reduced by coating the grating facets with a reflective metal.

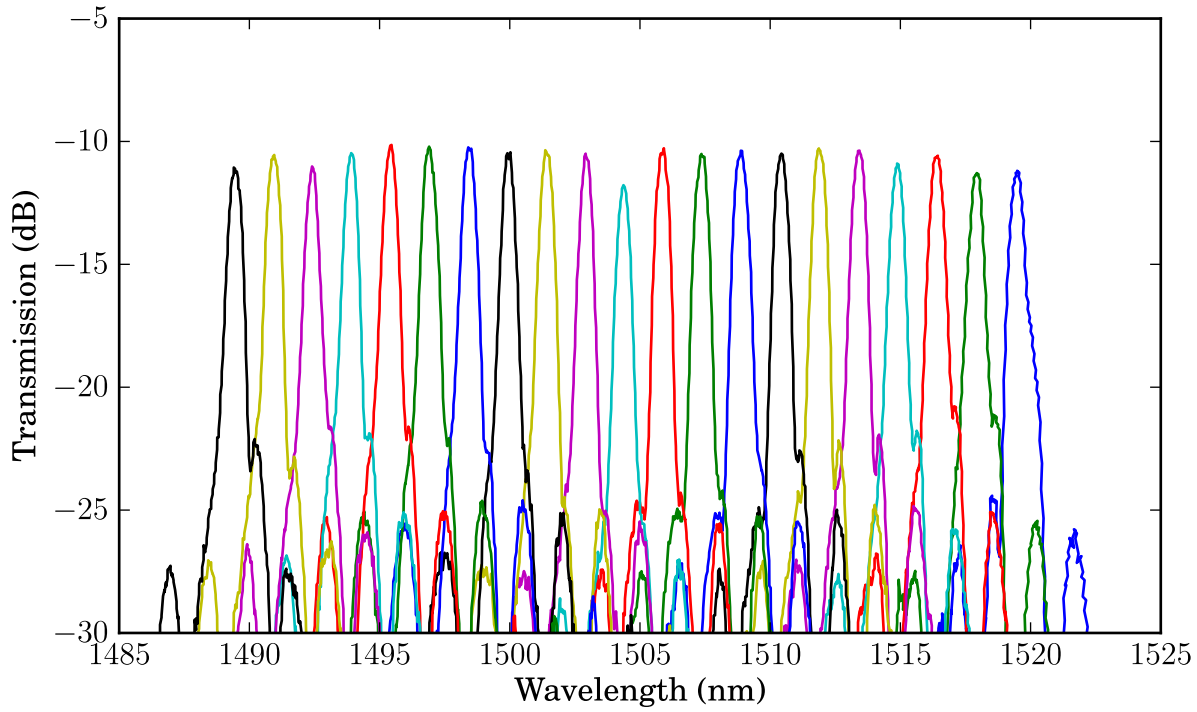

Figure 2.13.2: Transmission spectra of 21 channels of Rowland planar diffraction grating spectrometer.

In conclusion, we demonstrate a one point stigmatic Rowland grating WDM with 21 channels, 1 nm channel spacing and better than -10 dB crosstalk. Since the free spectral range is greater the 100 nm, by adding additional output waveguides it is possible to construct a WDM that covers whole C-band.

Chapter 3

Ring enhanced spectrometer

"tous pour un, un pour tous"

-Alexandre Dumas

How can we use resonators to make spectrometer. An array of resonators can be used. But fabrication limits prevent its use without requiring individually tuning each resonator. Grating spectrometers uses a lot of space. Is there a middle way. Yes! we can use small free spectral range resonators and a grating spectrometer. The device described in this chapter was published on optics express and presented on the Conference of Lasers and Electro-Optics 2010 (CLEO) as a invited paper and received and honorable mention in the Maiman Student Paper Competition.

3.1 Device Theory

The principle of operation consists of using a resonator to pre-filter the light to be analyzed by a diffraction grating spectrometer as shown in figure 3.1.1. The resonator transmits only the resonant wavelengths. A diffraction grating spectrometer is then used to route light from different resonances into distinct output channels. The net effect is that the final resonator and diffraction grating spectrometer line width will be equal to the resonator line width. On silicon ring resonators cladded with silicon dioxide, line width as narrow as 30 pm are routinely achieved[ref]. Therefore, enabling the possibility of creating 30 pm resolution spectrometers.

To achieve this, the resonator and the spectrometer must be designed so that the channel spacing of the diffraction grating spectrometer matches the ring resonator FSR.

The spectrometer must be designed so that each output channel only allows to transmit a single resonance. Therefore the spectrometer channel spacing must be equal to the resonator FSR.

The spectral resolution of the composed resonator and spectrometer can be estimated as follows.

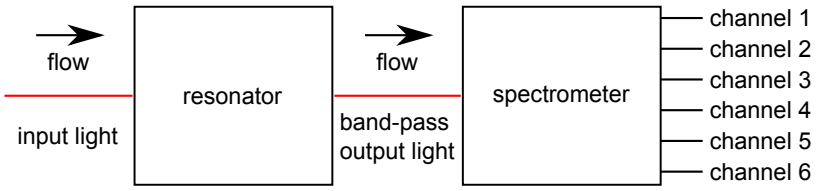

Figure 3.1.1:

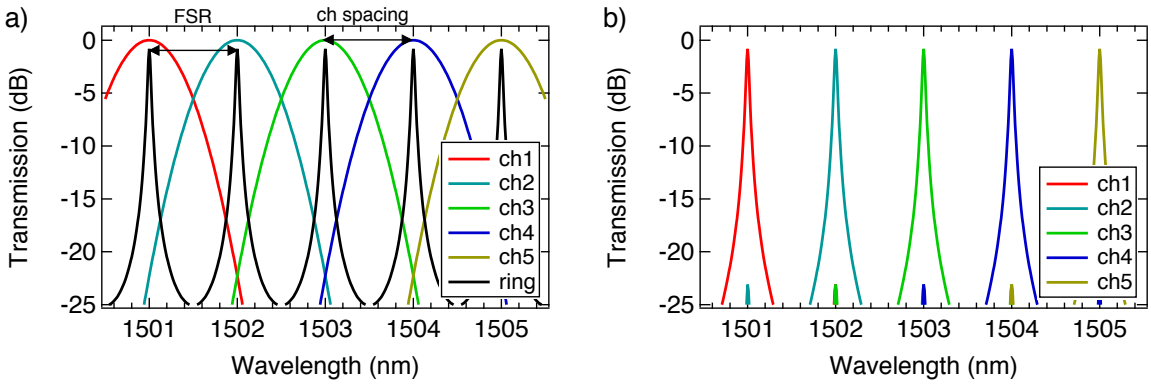

Figure 3.1.2:

The transmission spectrum of the composed resonator and spectrometer is the product of the resonator and spectrometer transmission spectrum, as shown in figure 3.1.2.a.

In the described configuration

3.1.1 Crosstalk

3.2 Design

We design the DG spectrometer using the Rowland architecture. To reduce spherical aberration, a non-uniform groove spacing is employed [20]. Metal heaters are added above the silicon layer [21] to align the resonator and spectrometer transmission combs using the thermo-optic effect in silicon. The diffraction grating spectrometer contains 25 channels with spacing of 1 nm. To match the ring resonator FSR to the DG spectrometer channel spacing we use an 83.5 m radius ring with waveguide cross-section of 450 x 250 nm. The FSR changes with wavelength according to $2\lambda/(n_g L)$, but considering a slight positive group velocity dispersion ($\partial n_g/\partial\lambda \approx 3.6 \times 10^{-3}\text{nm}^{-1}$) this change is extremely small: the total change in FSR across the range of operation (25 nm) is approximately 1% for light polarized in the plane of the device (TE polarization).

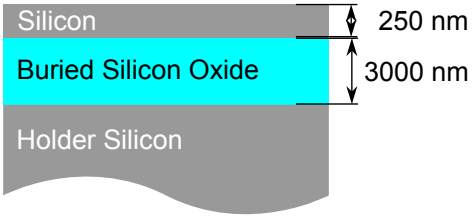

Figure 3.3.1:

3.3 Fabrication

The fabrication was done in the Cornell Nanoscale Facility (CNF), http://www.cnf.cornell.edu. A research micro-fabrication laboratory, funded in part by the National Science Foundation (NSF) and by its users. The research facility counts with state of the art electron beam lithography writer.

We fabricate the device using a CMOS compatible process. We start with a silicon-on- insulator (SOI), manufactured by Soitec (http://www.soitec.com) wafer with a 250 nm top silicon layer and a 3 μm buried oxide layer. A 60 nm layer of SiO_2 is deposited using high-temperature low-pressure chemical vapor deposition (HTO) to be used as a hard mask. The grating, ring and waveguides are defined by e-beam lithography on a PMMA resist mask. The pattern is transferred to the oxide layer using a CHF_3/O_2 reactive ion etch (RIE). The silicon layer is etched using chlorine RIE. A layer of 160 nm of SiO_2 is deposited using HTO to conformally fill the 100 nm gaps in the waveguide to ring coupling, then 1 μm of SiO_2 is deposited using plasma enhanced chemical vapor deposition to clad the device. We define the heaters using photolithography (using SPR955CM and LOR5A resists) and then deposit a NiCr film. After lift-off, t plahe wafer is diced and polished for optical testing.

3.4 Testing

We measure the device transmission spectrum by coupling laser light from a tunable laser into the input waveguide using a lensed fiber and measuring the transmitted power as a function of wavelength. The input light is TE polarized and the output light is collected using a microscope objective and filtered for the TE polarization before detection. We achieve a channel FWHM of 0.05 nm across 10 different channels of the composed ring and EDG spectrometer, which represents a decrease in the channel width by 10 times compared with the DG spectrometer alone. This channel width corresponds to a quality factor of Q = $\lambda/\Delta\lambda$= 30000.

Figure 3(b) shows the device transmission. The transmission is normalized to the ring through port power level to eliminate coupling losses. The device insertion loss varies between -18 and -23

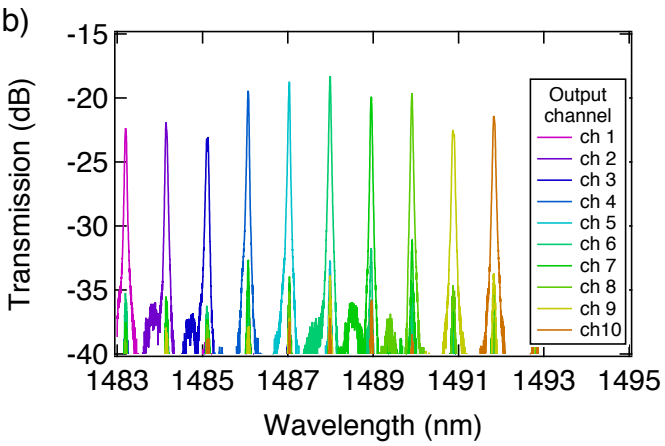

Figure 3.4.1:

dB, where -10 dB is due to the Fresnel reflection of the diffraction grating and can be eliminated by coating it with a metal or using Bragg reflectors [9]. Other losses are attributed to stitching in the waveguide definition during e-beam lithography. A small mismatch between the resonator FSR (0.97 nm) and the DG spectrometer channel spacing (1 nm) cause a misalignment between the resonance and the DG spectrometer channel that builds up from one channel to the next in a Vernier effect. The outcome is a misalignment between the 11th spectrometer channel and the 11th ring resonance. Therefore only 10 of the 25 channels on the DG spectrometer are used. This issue can be eliminated by more detailed characterization of fabrication.

3.5 Increasing Channel Density

change of refractive index with temperature

- ring tuning

-spectrometer tuning

Serializing devices either spatially or in time can increase the spectrometer channel density. The space serialization approach consists of using multiple combined ring-DG spectrometers, so that the input of a spectrometer is connected to the through port of the previous device, as shown in Fig. 4(a). The peak wavelength of each spectrometer is shifted relative to the others. The number of devices needed in order to achieve the a spectral density where the channels are separated by $\Delta\lambda_{FWHM}$, is equal to the DG spectrometer channel width divided by $\Delta\lambda_{FWHM}$. In spite of the area increase, this approach is still more compact than using a traditional diffraction grating spectrometer since in this proposed approach the area increases linearly with resolution as opposed to quadratic in traditional DGs.

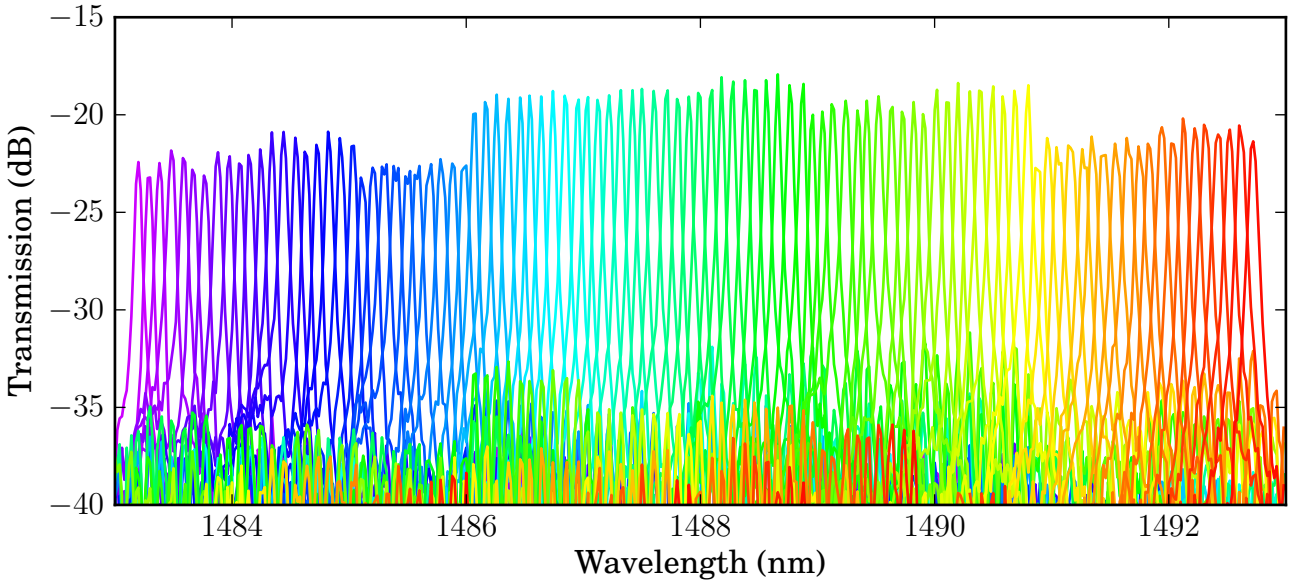

Figure 3.5.1:

In time serialization, Fig. 4(b), only a single combined spectrometer is used and the output spectrum is measured several times. In each measurement the device transmission spectrum is shifted. Notice that this approach also requires active tuning of the ring and the EDG spectrometer. By applying the time serialization technique we were able to reduce the channel spacing from 0.97 nm to 0.097 nm, and were able to measure 100 channels using the device.

A zoom in on the series of channels is depicted in Fig. 6 (a). Figure 6 (b) shows a density plot where each horizontal line corresponds to the transmission spectrum of each channel. Notice that the overlap of the residual transmission from the DG spectrometer with the neighboring resonances can be seen in the side diagonal lines, and their transmissions are at least 10 dB lower than the peak (main diagonal line).

Cross talk from neighboring channels

dfsdfasd

3.6 Effect of transmission spectrum lineshape

convolution relation

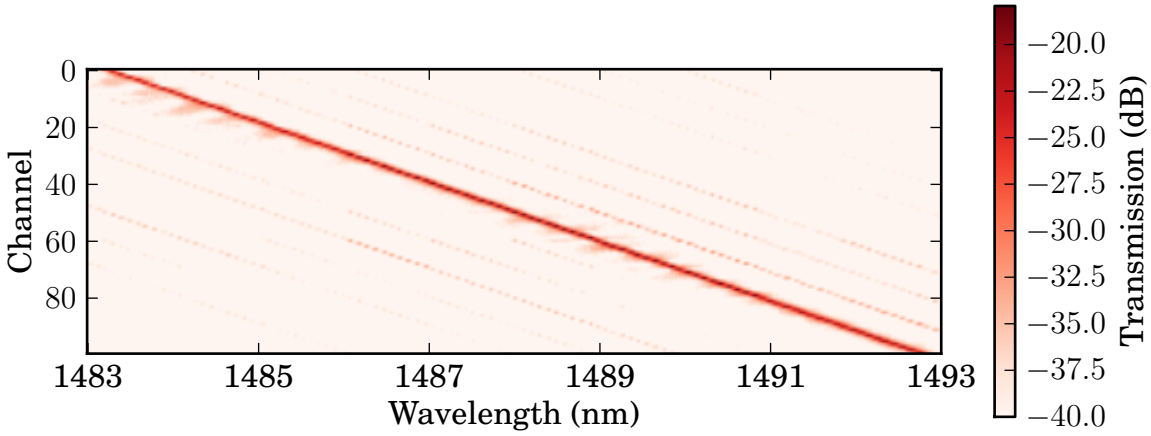
Channel
0
20
40
60
80
1483
1485
1487
1489
1491
1493
Wavelength (nm)
−20.0
−22.5
−25.0
−27.5
−30.0
−32.5
−35.0
−37.5
−40.0
Transmission (dB)

Figure 3.5.2:

Appendix I

For numerical computations some further simplifications can be done to the model described on section 2.10.

$$\begin{cases} P_x = I_x - y \sin \iota \\ P_y = I_y + y \cos \iota \end{cases}$$

$$\begin{cases} P'_x = I_x + r \cos (\iota + \alpha) \\ P'_y = I_y + r \sin (\iota + \alpha) \end{cases}$$

$$\begin{cases} P'_x = P_x + r' \cos (\iota + \alpha') \\ P'_y = P_y + r' \sin (\iota + \alpha') \end{cases}$$

$$\begin{cases} P'_x = I_x - y \sin \iota + r' \cos \alpha' \\ P'_y = I_y + y \cos \iota + r' \sin \alpha' \end{cases}$$

$$r_1 = |P' - I|$$

$$r'_1 = |P' - P|$$

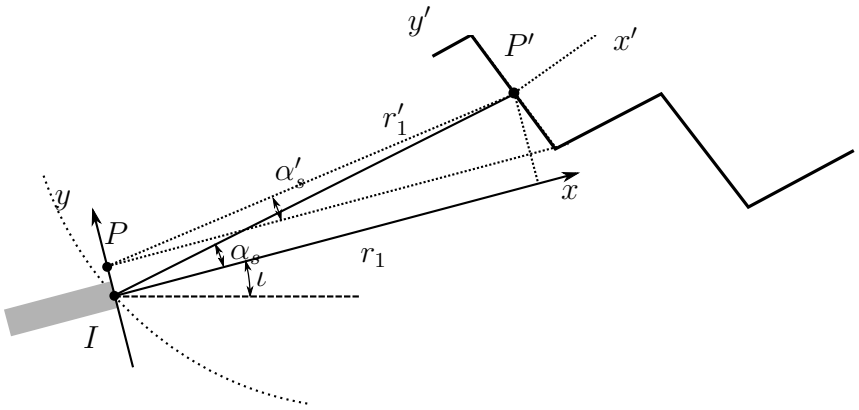

Figure 3.6.1:

$$r'^2 = \left(P'_y - P_y\right)^2 + P'^2_x$$

$$r' = \sqrt{\left(r\sin\alpha - P_y\right)^2 + r\cos^2\alpha}$$
$$r' = \sqrt{r^2 - 2P_y r\sin\alpha + P_y^2}$$
$$r' = r\sqrt{1 - 2\frac{P_y}{r}\sin\alpha + \left(\frac{P_y}{r}\right)^2}$$
$$r' = r\left[1 - \frac{P_y}{r}\sin\alpha + O\left(2\right)\right]$$

for

$$\cos\alpha' = \sqrt{1-\sin^2\alpha'} = \sqrt{1 - \left(\frac{P'_y - P_y}{r'}\right)^2} = \sqrt{1 - \left[\frac{r\left(\sin\alpha - \frac{P_y}{r}\right)}{r\left(1 - \frac{P_y}{r}\sin\alpha\right)}\right]^2} \approx \cos\alpha + \frac{P_y}{r}\sin\alpha\cos\alpha$$

$$\frac{1}{\sqrt{r'}} = \frac{1}{\sqrt{r}}\frac{1}{1 - \frac{P_y}{r}\sin\alpha + O\left(2\right)} \approx \frac{1}{\sqrt{r}}\left(1 + \frac{P_y}{2r}\sin\alpha\right)$$

Putting all together:

$$E_{inc} = \frac{1}{2}\sqrt{\frac{n_{eff}}{\lambda}}\int E_{wg}\left(y\right)\frac{e^{-ikr'}}{\sqrt{r'}}\left(1+\cos\alpha'\right)dP_y$$

dsd $E_{wg}\left(y\right) = E\exp\left[-4\ln 2\left(\frac{P_y}{w}\right)^2\right]$

$$E_{inc} = \frac{1}{2}\sqrt{\frac{n_{eff}}{\lambda}}\int E_{wg}\left(y\right)\frac{e^{-ikr+ikP_y\sin\alpha}}{\sqrt{r}}\left(1+\frac{P_y}{2r}\sin\alpha\right)\left(1+\cos\alpha+\frac{P_y}{r}\sin\alpha\cos\alpha\right)dP_y$$

$$E_{inc} = \frac{1}{2}\sqrt{\frac{n_{eff}}{\lambda}}\int E\exp\left[-4\ln 2\left(\frac{P_y}{w}\right)^2\right]\frac{e^{-ikr+ikP_y\sin\alpha}}{\sqrt{r}}\left(1+\frac{P_y}{2r}\sin\alpha\right)\left(1+\cos\alpha+\frac{P_y}{r}\sin\alpha\cos\alpha\right)dP_y$$

$$E_{inc} = \frac{1}{2}\sqrt{\frac{n_{eff}}{\lambda}}\frac{E}{\sqrt{r}}\int\exp\left[-4\ln 2\left(\frac{P_y}{w}\right)^2\right]e^{-ikr}e^{-ikP_y\sin\alpha}\left(1+\cos\alpha+\frac{P_y}{r}\left(\frac{1}{2}+\frac{3}{2}\sin\alpha\cos\alpha\right)+\frac{1}{2}\left(\frac{P_y}{r}\right)^2\sin^2$$

$$E_{inc} = \frac{1}{2}\sqrt{\frac{n_{eff}}{\lambda}}\frac{E}{\sqrt{r}}e^{-ikr}\left\{\left(1+\cos\alpha\right)\int\exp\left[-4\ln 2\left(\frac{P_y}{w}\right)^2\right]e^{-ikP_y\sin\alpha}dP_y + \frac{1}{r}\left(\frac{1}{2}+\frac{3}{2}\sin\alpha\cos\alpha\right)\int\exp\left[-4\ln\right.\right.$$

Appendix II

3.7 Numerical calculation

The simulatior is divided in two main files. The spectrometer.py and WavePropagation.py.

spectrometer.py contains the classes necessary to build the spectrometer.

WavePropagation.py contains the implementation of the Kirchhoff-Huygens integrals that are going to be applied over the spectrometer build using spectrometer.py

$$U(P) = \int_{\mathbb{Q}} \frac{e^{\mathrm{i}kr}}{\sqrt{kr}} \left[\frac{ikU(Q)}{2} \cos(r,n) - \frac{\partial U(Q)}{\partial n} \right] dS$$

$$\frac{\partial U(P)}{\partial m} = \frac{ik}{2} \int_{\mathbb{Q}} \frac{e^{\mathrm{i}kr}}{\sqrt{kr}} \left[U(Q) \frac{ik}{2} \cos(r,n) - \frac{\partial U(Q)}{\partial n} \right] \cos(r,m)\, dS$$

3.8 Approximations

If the aperture $\mathbb{Q}$ is much smaller than r, then we can consider that $\cos(r,m)$ does not vary a lot in the integral, therefore we can pull it outside the integral, which convert the integral to $U(P)$.

center

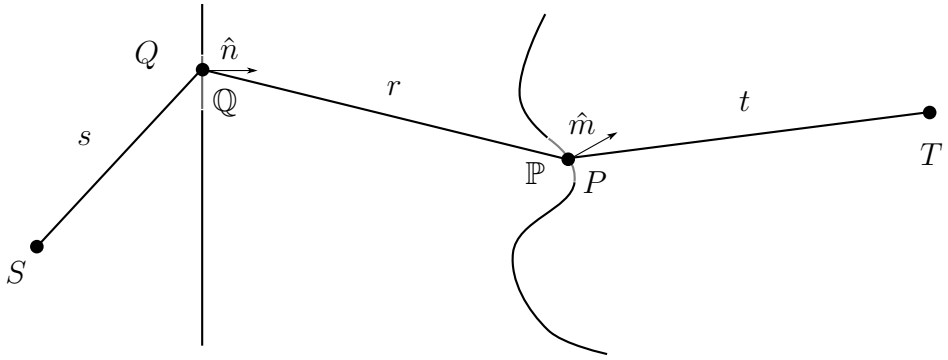

Figure 3.7.1:

We therefore can simplify the equations to

$$\begin{cases} U(P) = \int_{\mathbb{Q}} \frac{e^{\mathrm{i}kr}}{\sqrt{kr}} \left[\frac{ikU(Q)}{2} \cos(r,n) - \frac{\partial U(Q)}{\partial n} \right] dS \\ \frac{\partial U(P)}{\partial m} = \frac{ik}{2} \cos(r,m)\, U(P) \end{cases}$$

$$\frac{\partial U(P)}{\partial m} = \frac{ik}{2} \cos(r,m) \int_{\mathbb{Q}} \frac{e^{\mathrm{i}kr}}{\sqrt{kr}} \left[U(Q) \frac{ik}{2} \cos(r,n) - \frac{\partial U(Q)}{\partial n} \right] dS = \frac{ik}{2} \cos(r,m)\, U(P)$$

Appendix III

Cossine does not vary much

We can enclose $\mathbb{Q}$ by a circule of radius q centered at Q_C, we therefore can write any point of Q by $Q = Q_C + v$ where $|v| < q$. And we define $\vec{r'} = P - Q_C$

$$\cos(r, m) = \frac{\vec{r} \cdot \hat{m}}{r} = \frac{(P - Q) \cdot \hat{m}}{|P - Q|}$$

$$\cos(r, m) = \frac{\vec{r} \cdot \hat{m}}{r} = \frac{(P - Q_C - v) \cdot \hat{m}}{|P - Q_C - v|} = \frac{\vec{r'} \cdot \hat{m} - \vec{v} \cdot \hat{m}}{|\vec{r'} - \vec{v}|} = \frac{\vec{r'} \cdot \hat{m}}{|\vec{r'} - \vec{v}|} - \frac{\vec{v} \cdot \hat{m}}{|\vec{r'} - \vec{v}|} = \frac{r' \cos(r', m)}{\left|\vec{r'} - \vec{v}\right|} - \frac{v \cos(v, m)}{\left|\vec{r'} - \vec{v}\right|}$$

$$\left|\vec{r'} - \vec{v}\right| = \sqrt{r'^2 + v^2 + r' v \cos(r, v)} = r' \sqrt{1 + \frac{v^2}{r'^2} + \frac{v}{r'} \cos(r, v)}$$

$$\cos(r, m) = \frac{\cos(r', m)}{\sqrt{1 + \frac{v^2}{r'^2} + \frac{v}{r'} \cos(r, v)}} - \frac{v}{r'} \frac{\cos(v, m)}{\sqrt{1 + \frac{v^2}{r'^2} + \frac{v}{r'} \cos(r, v)}}$$

since $v < q \ll r'$, then at first approximation $\cos(r, m) = \cos(r', m) + O\left(\frac{q}{r'}\right)$

Bibliography

[1] J Brouckaert, W Bogaerts, P Dumon, D Van Thourhout, and R Baets. Planar concave grating demultiplexer fabricated on a nanophotonic silicon-on-insulator platform. *Journal of Lightwave Technology*, 25(5):1269–1275, 2007.

[2] L Gabrielli, J Cardenas, C Poitras, and M Lipson. Silicon nanostructure cloak operating at optical frequencies. *Nature Photonics*, Jan 2009.

[3] HA Rowland. Xxix. on concave gratings for optical purposes. *Philosophical Magazine Series 5*, 16(99):197–210, 1883.

[4] H Takahashi, S Suzuki, K Kato, and I Nishi. Arrayed-waveguide grating for wavelength division multi/demultiplexer with nanometre resolution. *Electronics letters*, 26(2):87–88, 1990.